ChemPubSoc Europe

DOI: 10.1002/cssc.201802845

CHEMSUSCHEM Full Papers

Multilayered Hematite Nanowires with Thin-Film Silicon Photovoltaics in an All-Earth-Abundant Hybrid Tandem Device for Solar Water Splitting

Félix Urbain,*[a] Pengyi Tang,[a, b] Vladimir Smirnov,[c] Katharina Welter,[c] Teresa Andreu,[a, d] Friedhelm Finger,[c] Jordi Arbiol,[b, e] and Joan Ramón Morante[a, f]

The concept of hybrid tandem device structures that combine metal oxides with thin-film semiconducting photoabsorbers holds great promise for large-scale, robust, and cost-effective bias-free photoelectrochemical water splitting (PEC-WS). This work highlights important steps toward the efficient coupling of high-performance hematite photoanodes with multijunction thin-film silicon photocathodes providing high bias-free photocurrent density. The hybrid PEC-WS device is optimized by testing three types of multijunction silicon photocathodes with the hematite photoanode: amorphous silicon (a-Si:H) tandem: a-Si:H/a-Si:H and triple junction with microcrystalline silicon (μc-Si:H): a-Si:H/a-Si:H/μc-Si:H and a-Si:H/μc-Si:H/μc-Si:H. The results provide evidence that the multijunction structures offer high flexibility for hybrid tandem devices with regard to tunable photovoltages and spectral matching. Furthermore, both photoanode and photocathode are tested under various electrolyte and light concentration conditions, respectively, with respect to their photoelectrochemical performance and stability. A 27% enhancement in the solar-to-hydrogen conversion efficiency is observed upon concentrating light from 100 to 300 mW cm^{-2}. Ultimately, bias-free water splitting is demonstrated, with a photocurrent density of 4.6 mA cm^{-2} (under concentrated illumination) paired with excellent operation stability for more than 24 h of the all-earth-abundant and low-cost hematite/silicon tandem PEC-WS device.

Introduction

Recently, photoelectrochemical water splitting (PEC-WS) has been standing at the center of critical studies judging the technology against photovoltaics (PV)–electrolyzer systems with respect to cost, efficiency, and stability.[1–3] It still remains to be proven what PEC-WS devices promised to offer compared with other production routes for solar hydrogen: 1) reduced costs through a higher level of integration, 2) potentially higher solar-to-hydrogen (STH) efficiencies because of direct one-step conversion, and 3) stable operation by employing chemically robust materials.[4] Regarding these requirements, hematite photoelectrodes appear as ideal candidates for PEC-WS devices owing to their high natural abundance, low-cost, and scalable deposition, adequate bandgap energy for WS (≈2 eV), and photochemical robustness.[5] However, despite many years of extensive research, hematite photoelectrodes could not live up to their promises, mainly because of their low photovoltages, poor catalytic activity, and limited electrical conductivity. The present contribution aims to bring hematite back on track as a PEC-WS material by making use of its beneficial properties in combination with another earth-abundant and low-cost scalable photovoltaic material, namely, thin-film silicon. In this monolithic tandem configuration, we seek to provide enough photovoltage to drive the water-splitting reaction bias-free while ensuring a high photocurrent through good spectral matching of both light absorbers and improved catalytic properties for both the oxygen evolution reaction (OER) and hydrogen evolution reaction (HER). In particular, we combined an advanced hematite photoanode with multijunction thin-film silicon photocathodes. For the latter, we optimized the absorber layer sequence to reach the best photocurrent–photovoltage tradeoff upon coupling with the hematite absorber. The photoanode was composed of an indium-doped tin oxide (ITO) underlayer with Fe_2O_3 nanowires coated with a Fe_2TiO_5 (pseudobrookite) atomic layer and decorated with FeNiOOH nanodots,

[a] F. Urbain, P. Tang, T. Andreu, J. R. Morante
IREC, Catalonia Institute for Energy Research
Jardins de les Dones de Negre 1, 08930 Sant Adrià de Besòs, Barcelona, Catalonia (Spain)
E-mail: furbain@irec.cat

[b] P. Tang, J. Arbiol
Catalan Institute of Nanoscience and Nanotechnology (ICN2), CSIC and BIST
Campus UAB, Bellaterra, 08193 Barcelona, Catalonia (Spain)

[c] V. Smirnov, K. Welter, F. Finger
IEK-5 Photovoltaik
Forschungszentrum Jülich
52425, Jülich (Germany)

[d] T. Andreu
Universitat Politècnica de Catalunya
Jordi Girona 1-3, 08034 Barcelona, Catalonia (Spain)

[e] J. Arbiol
ICREA
Pg. Lluís Companys 23, 08010 Barcelona, Catalonia (Spain)

[f] J. R. Morante
Universitat de Barcelona
Martí i Franquès, 1, 08028 Barcelona, Catalonia (Spain)

Supporting Information and the ORCID identification number(s) for the author(s) of this article can be found under: https://doi.org/10.1002/cssc.201802845.

as reported recently by Tang et al.[6] By this integrated "one-chip" tandem approach, we circumvent the need for a counter electrode, which is physically separated from the photoelectrode and usually composed of expensive materials.[7] As a consequence, the approach presented herein allows the replacement of costly and scarce OER materials, such as RuO_2, by cost-effective and earth-abundant hematite nanostructures. Another advantage of the proposed dual-absorber architecture is that the water-splitting reactions occur directly at the semiconductor–liquid interface, which minimizes the number of junctions used, making the overall device simpler and potentially cheaper. Moreover, in contrast to previous approaches for unassisted PEC-WS using oxide-based hybrid tandem structures,[8–10] this study only investigated earth-abundant catalyst materials and analyzed the tandem system through robust stability testing. Furthermore, we introduced light concentration as an effective method to enhance the photoelectrochemical performance of both hybrid tandem partners to increase the achievable photocurrent density of the complete PEC-WS device.

Experimental Section

The fabrication of the ITO/Fe_2O_3/Fe_2TiO_5/FeNiOOH photoanode and the thin-film silicon multijunction photocathodes, as well as the optical, structural, and compositional characterization of both hybrid tandem partners, are described in detail in Section 1 of the Supporting Information.

For the (photo)electrochemical characterization, both photoelectrodes were analyzed by means of linear sweep measurements (VMP3 Bio-Logic multichannel potentiostat) conducted at a scan rate of 10 mV s^{-1} in a three-electrode setup using a Ag/AgCl (3 M KCl) reference electrode in aqueous NaOH electrolyte under ambient conditions. A 150 W AM 1.5G solar simulator (Solar Light Co., 16S-300-002 v4.0) was used as the light source, and the light density was calibrated by using a thermopile (Gentec-EO, XLPF12-3S-H2-DO) coupled with an optical power meter (Gentec-EO UNO). The intensity of the light source was adjusted to match concentrated illumination conditions from 100 to 300 mW cm^{-2} intensity, by varying the distance between the PEC-WS device and the solar simulator. For the hybrid tandem configuration both photoelectrodes were attached such that the glass sides of both respective substrates were in direct contact for good optical coupling. In the two-electrode configuration (chronoamperometry at 0 V applied bias) the complete PEC-WS device was sealed using thermoplastic resin paste surrounding the device except for the two 1 cm^2 apertures defining the active areas for the solar-driven OER and HER, respectively. We applied nickel-based HER catalysts in this study. Both photoelectrodes were electrically contacted on the respective FTO-coated glass substrates. Scheme 1 provides a depiction of the hybrid tandem device setup under operation.

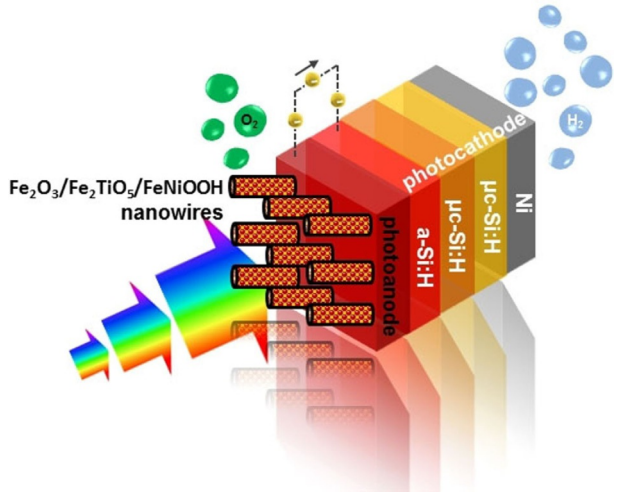

Scheme 1. The hybrid tandem device under operation. The OER is performed by the ITO/Fe_2O_3/Fe_2TiO_5/FeNiOOH multilayered nanowire photoanode and the HER is powered by a multijunction thin-film silicon photocathode and a Ni-based catalyst. The light enters through the photoanode, as depicted.

Results

Multilayered hematite nanowire photoanode

The TEM and high-resolution TEM (HRTEM) images of the hematite multilayer nanowires are shown in Figure 1 a and b, respectively. The coating of the Fe_2O_3 nanowire core by the pseudobrookite shell can be seen in Figure 1 d–f, deduced from the HRTEM image in Figure 1 b and the corresponding fast-Fourier-transform (FFT) spectrum in Figure 1 c. As demonstrated in Ref. [6], this atomic layer can effectively suppress the charge recombination at the semiconductor junction interface, and the ITO underlayer enhances the electrical conductivity of the photoanodes, resulting in a higher photocurrent density and an enhanced fill factor. The OER performance can be promoted by using FeNiOOH nanodots (Figure 1 b and Figure S1, Supporting Information), which were deposited on the nanowire surface by photo-electrodeposition. In this way, the number of active sites on the nanowire surface can be increased, which is conducive to accelerated OER kinetics at the semiconductor–electrolyte interface, resulting in photocurrent densities of up to 2.2 mA cm^{-2} at 1.23 V versus the reversible hydrogen electrode (RHE).[6] The electron energy loss spectroscopy (EELS) measurements of the as-developed nanowire structures on the FTO glass/ITO substrate can be found in Figure S2 of the Supporting Information.

Optical coupling of both tandem absorber partners

In the case of a dual-absorber tandem device, the photocathode should also fulfil particular requirements to enable unassisted overall water splitting: 1) it must provide enough additional photovoltage, 2) it should be compatible with catalysts for efficient and stable HER, and 3) it should possess an adequate bandgap energy for efficient spectral matching with the hematite light absorber used for the OER. All these tasks can be performed using multijunction thin-film silicon photovoltaics made of hydrogenated amorphous (a-Si:H) and microcrystalline silicon (μc-Si:H) films. As already shown elsewhere,[7,11,12] "stacking" of a-Si:H and μc-Si:H absorber layers in monolithic multijunction solar cells (in contrast to crystalline silicon solar cells) allows highly precise adjustment of the photovoltaic parameters such as the photovoltage without complex electrical

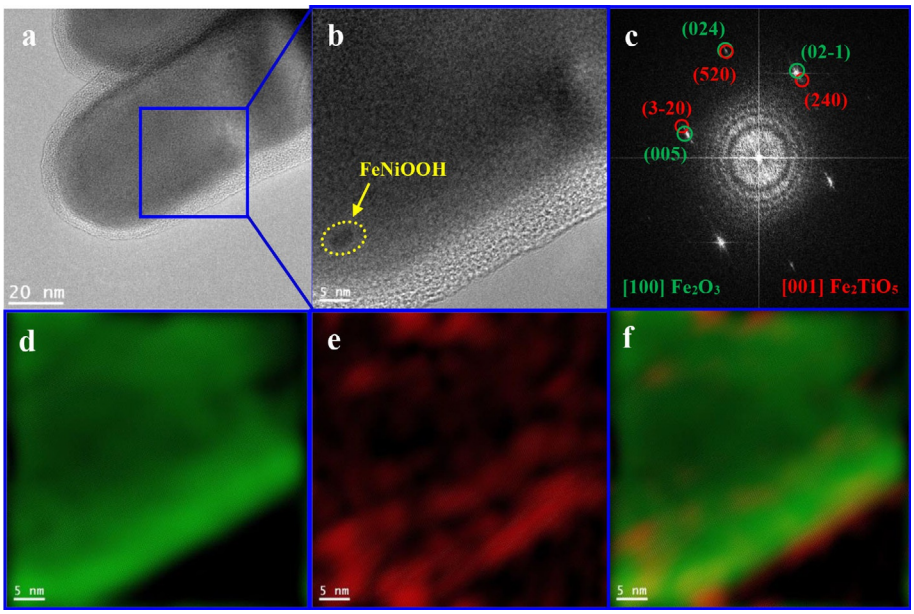

Figure 1. a) Low-magnification TEM image of a multilayer nanowire. b) High-resolution TEM image of the blue squared area showing the hierarchical structure of the nanowire composite and the decoration of FeNiOOH nanodots, which are shown in more detail in Figure S1 (Supporting Information). c) Corresponding FFT spectrum of (b), indicating that the nanowire is composed of hematite and pseudobrookite, visualized along the [100] and [001] directions, respectively. d) Phase map (green) of Fe_2O_3. e) Phase map (red) of Fe_2TiO_5. f) Mixed phase map of (d) and (e). All phase maps were obtained from (b) after mask filtering the corresponding spots for each of the crystal phases in (c) and obtaining their corresponding inverse fast-Fourier-transform (IFFT) image. The IFFT RGB composite image in (f) reveals the coating of pseudobrookite on the surface of the hematite nanowire.

connections, which would limit the practical application of PEC-WS systems in terms of their compactness and customizability. Additionally, the thin-film silicon technology benefits from earth-abundance, low material consumption (absorber layer thickness below 3 μm), light weight, low-cost production, facile large-scale deposition, and the possibility of combination with a wide range of HER catalysts.

We investigated three types of multijunction thin-film silicon cells for combination with the hematite photoanode: a-Si:H/a-Si:H, a-Si:H/a-Si:H/μc-Si:H, and a-Si:H/μc-Si:H/μc-Si:H. The layer thicknesses for the individual a-Si:H and μc-Si:H sub-cells of the selected solar cells were optimized with respect to high photovoltage and good current matching. It was shown that the photovoltage can be tuned systematically between 1.8 and 2.3 V with photovoltaic conversion efficiencies of up to 13.6%. Therefore, the thin-film silicon multijunction solar cells offer high flexibility for usage as photocathodes in hybrid dual-absorber devices. Details on the preparation and application as photocathodes of the tested multijunction cells can be found in Refs. [7] and [11], respectively, and in the Supporting Information (Section 1). In the hybrid tandem configuration for PEC-WS proposed herein, the photoanode was placed before the photocathode because the optical bandgap energy of hematite is higher than that of thin-film silicon.[13] The quantum efficiencies (*QE*) of the tested thin-film silicon solar cells, with and without the hematite photoanode as filter, are shown in Figure 2 (left *y*-axis). These measurements provide insights into the optical absorption and carrier extraction efficiency of the photocathode in the hybrid tandem configuration, that is, upon the light first passing through the hematite absorber and then entering the thin-film silicon material. The *QE* measurements and calculations are described in detail in the Supporting Information (Section 2).

The *QE* of the multijunction thin-film silicon sub cells with the hematite photoanode filter (purple curves) were calculated on the basis of the measured *QE* (dashed black curves) and the measured transmission characteristic of the hematite photoanode filter, shown in Figure 2 (right *y*-axis). Please note that the calculated and measured *QE* of the filtered multijunction solar cells were in very good agreement for the a-Si:H/a-Si:H solar cell, as shown in Figure S3 (Supporting Information), which is why we used the calculated *QE* for all investigated cell types. As is apparent from Figure 2 (left *y*-axis), the hematite material significantly reduced the *QE* of the three tested thin-film silicon structures over the whole investigated wavelength range, that is, 350–1100 nm. The incoming light with wavelengths below 550 nm was completely absorbed by the photoanode material. As the sub-cells of the multijunction devices are electrically connected in series, the overall photocurrent of the photocathode will be defined by the smallest *QE* of the individual sub-cells. The limiting sub-cell for each cell type is highlighted by a green filling in Figure 2. A magnified view of each of the limiting *QE*s is shown in Figure S4 (Supporting Information), including the respective calculated photocurrent densities. The highest limiting sub-cell *QE* was provided by the a-Si:H/μc-Si:H/μc-Si:H solar cell with the hematite filter (Figure 2, bottom). In this configuration, the first a-Si:H absorber layer, for which the light absorption was most affected by the hematite filter in all tested cells, had a thickness of 160 nm, and thus was thicker than the a-Si:H top cells in the a-Si:H/a-Si:H, and a-Si:H/a-Si:H/μc-Si:H configuration, respectively, with a thickness of 90 nm for both solar cells. This im-

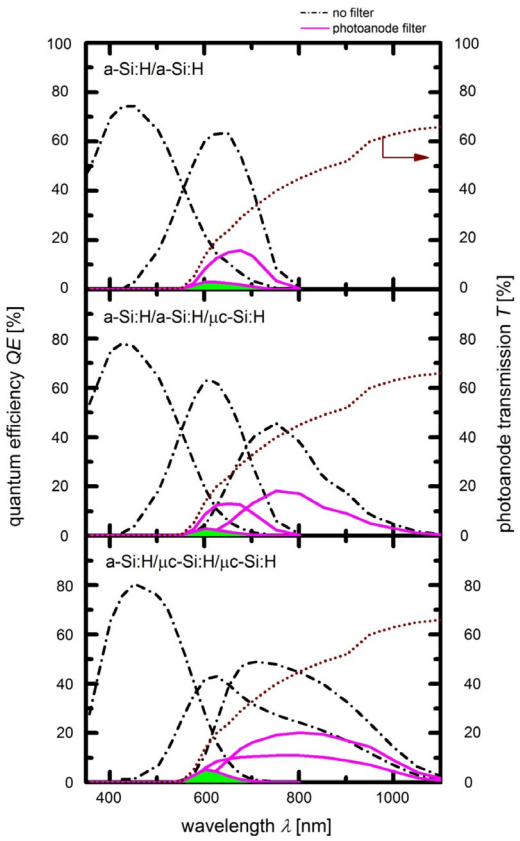

Figure 2. Left *y*-axis: *QE* for the three investigated thin-film silicon multijunction photocathodes: a-Si:H/a-Si:H, a-Si:H/a-Si:H/μc-Si:H, and a-Si:H/μc-Si:H/μc-Si:H. The dotted black lines show the measurements without filter and the purple lines show the calculated quantum efficiencies with the hematite placed before the silicon photocathodes. The calculations were based on the transmission measurement of the hematite photoanode, plotted on the right *y*-axis. For the convenience of the reader, the limiting sub-cell quantum efficiencies are indicated in green; these are shown in a magnified view in Figure S4 (Supporting Information).

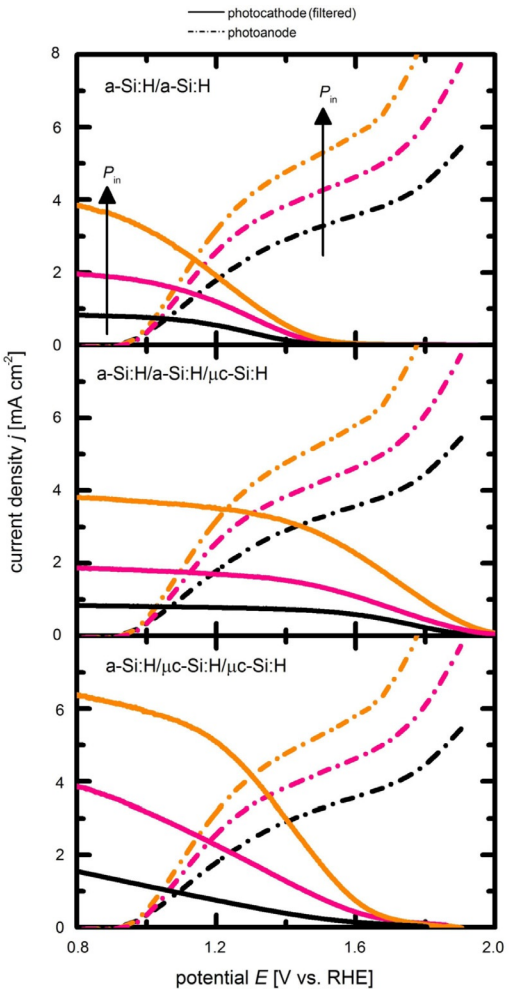

Figure 3. Linear-sweep measurements of the three investigated thin-film silicon multijunction photocathodes (with hematite filter, solid lines): a-Si:H/a-Si:H, a-Si:H/a-Si:H/μc-Si:H, and a-Si:H/μc-Si:H/μc-Si:H, and the hematite photoanode (dashed lines) as a function of the illumination intensity (P_{in}). The measurements were conducted at 100 (black lines), 200 (purple lines), and 300 mW cm^{-2} (orange lines) in 1 M NaOH electrolyte solutions using a Ag/AgCl reference electrode (3 M KCl). A Ni foil was used as the HER catalyst for the tested photocathodes.

plied a better absorption of the incoming light and consequently a higher sub-cell *QE*. Increasing the thickness of the a-Si:H top cell layer beyond 160 nm would cause a spectral mismatching of the individual sub-cell photocurrent densities, thus impairing its performance. Nevertheless, beyond the aim of this study (to present a proof of concept of a high-current PEC-WS device), upcoming studies should focus on the optimization of the layer stack sequences and thicknesses, respectively, especially adapted for the combination with hematite-based light-absorbers. Moreover, other metal-oxide photoanodes could be combined with a multijunction thin-film silicon photocathode for PEC-WS. One salient candidate is $BiVO_4$ (band-gap energy ≈2.3–2.4 eV), which, however, still suffers from poor electrochemical stability.

Photoelectrochemical performance under light concentration

The photoelectrochemical performance of the filtered multijunction silicon photocathodes from Figure 2 and the hematite photoanode, respectively, is presented in Figure 3 (black curves). A nickel (Ni) foil on the surface of the silicon photocathodes served as the HER catalyst (see experimental details in the Supporting Information). As expected from the *QE* measurements, the filtered a-Si:H/μc-Si:H/μc-Si:H photocathode (Figure 3, bottom) exhibited the highest photocurrent density among the tested silicon photocathodes of 1.8 mA cm^{-2} at 0.8 V versus RHE. Despite a lower onset potential compared with the a-Si:H/a-Si:H/μc-Si:H photocathode and despite the lowest fill factor among the tested photocathodes (black solid curves), the crossing point of the a-Si:H/μc-Si:H/μc-Si:H photocathode with the hematite photoanode current–voltage (*j*–*V*) curve (dashed black curve) lay at the highest photocurrent density of 1.1 mA cm^{-2}, from which an estimated STH efficiency of 1.35% can be calculated. The photocurrent densities at the crossing point for the a-Si:H/a-Si:H and a-Si:H/a-Si:H/μc-Si:H photocathodes were 0.7 and 0.9 mA cm^{-2}, respectively. Besides the fact that all tested silicon photocathodes provided enough

photovoltage to potentially enable bias-free water splitting using the hematite photoanode, the results of Figures 2 and 3, respectively, furthermore demonstrate the high flexibility of multijunction thin-film silicon solar cells in terms of the adjustment of the photovoltage and photocurrent in a dual-absorber device.

Nevertheless, to reach the target hydrogen production required in industry or domestic usage, it is crucial to identify methods to increase the bias-free photocurrent without expensive upscaling. The most efficient and straightforward method to achieve this involves increasing the available illumination intensity for the hybrid tandem device by light concentration.[14,15] The effect of concentrated light illumination on the silicon photocathodes (solid curves) and on the photoanode (dashed curves) is also shown in Figure 3. We tested concentration factors of 2 and 3, giving illumination intensities (P_{in}) of 200 (purple curves) and 300 mW cm^{-2} (orange curves), respectively. Please note that the light concentration was achieved by approaching the hybrid tandem to the sun simulator, and thus, some small deviations from the exact concentration factors might be introduced. The strongest increase with light concentration in the photocurrent density at the crossing point of the photocathode and the photoanode *j–V* characteristics was obtained with the hematite/a-Si:H/μc-Si:H/μc-Si:H configuration. At 300 mW cm^{-2} illumination intensity, an estimated bias-free current density of 4.2 mA cm^{-2} was deduced, corresponding to an STH efficiency of 1.72% (calculated). Hence, a 27% enhancement in the STH conversion efficiency can be achieved by increasing the illumination intensity from 100 to 300 mW cm^{-2}, stemming from an enhanced performance of both the photoanode and the filtered photocathode with increased P_{in}. As apparent from the *j–V* curves in Figure 3, the onset potential of the photoelectrodes was not affected significantly by the increased P_{in}. The value of the onset potential, besides catalysis, also depends on the internal structure of the photoabsorbing material, that is, on the recombination and charge-transfer processes.[16] Additionally, the photoelectrodes were heated up during concentrated illumination, which usually results in a slight decrease in the photovoltage.[15] Recombination and temperature effects therefore might have hampered a more pronounced increase in the onset potential, as one would expect from semiconductor devices upon increased illumination intensity, that is, in the presence of more photogenerated charge carriers. The influence of higher temperatures on the *j–V* characteristics of the hematite photoanode is presented in Figure S5 (Supporting Information). The increased temperature conditions, besides the expected overall enhanced photoelectrochemical performance of the photoanode, resulted in a negligible small shift of the onset potential, which is consistent with the aforementioned assumptions.

The estimated bias-free photocurrent densities as well as the deduced estimated STH efficiencies for all investigated configurations as a function of the incident light intensity can be found in Figure 4. For the hematite/a-Si:H/μc-Si:H/μc-Si:H configuration, an increase in P_{in} not only augmented the photocurrent density but also significantly increased the fill factor of the filtered a-Si:H/μc-Si:H/μc-Si:H photocathode (Figure 3, bottom). This effect might be related to the fact that the recombination junctions at the different thin-film silicon sub-cell interfaces are very sensitive to light concentration, in particular at μc-Si:H/μc-Si:H junctions.[17] With the hematite photoanode as filter, this junction received a significantly reduced amount of light, which is why fewer charge carriers were photogenerated, causing a higher resistance of the junction at 100 mW cm^{-2} illumination intensity. By increasing the light concentration, losses related to the junction resistance were reduced, resulting in a better fill factor at 300 mW cm^{-2}. This effect was also observable in the photovoltaic configuration (without electrolyte) as shown in Figure S6 (Supporting Information). Moreover, as mentioned above, the increased light illumination increased the temperature of the surrounding electrolyte, which is conducive to improved electrochemical reaction kinetics, significantly reducing recombination losses owing to improved charge-transfer kinetics at the photoelectrode/electrolyte interface.[18]

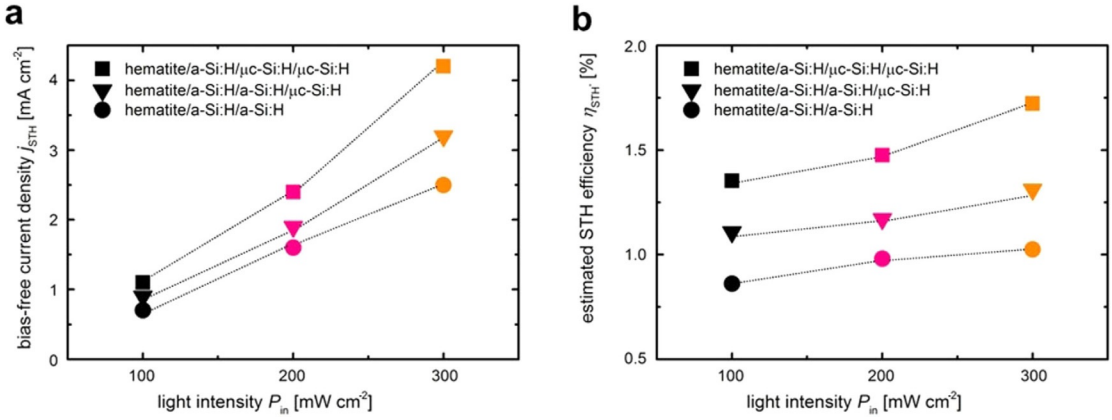

Figure 4. a) Photocurrent densities at the crossing points (i.e., estimated bias-free current densities) of the *j–V* characteristics of the filtered multijunction thin-film silicon photocathodes and the hematite photoanode, respectively, as a function of the incident light intensity P_{in}, obtained from Figure 3. b) Estimated STH efficiencies calculated from the values in (a) as a function of the incident light intensity P_{in}.

HER catalysis optimization

To further enhance the efficiency of the hybrid tandem device, the catalysis, especially the HER, was considered. First, we tested higher electrolyte concentrations of the NaOH solution. The effect of NaOH concentrations of up to 6 M on the *j–V* characteristics of the filtered a-Si:H/μc-Si:H/μc-Si:H photocathode and the hematite photoanode, respectively, at 300 mW cm^{-2} illumination intensity can be found in Figure S7a (Supporting Information). The results suggest that the photocurrent density at the crossing point of the photocathode and photoanode *j–V* curves, that is, the estimated bias-free photocurrent, remained unchanged with increasing NaOH concentration (Figure S7b). Therefore, we chose 1 M NaOH solution as the best choice to achieve efficient and stable operation of the hybrid tandem device, avoiding issues such as pitting corrosion or delamination of the active layers.

The second aim was to enhance the HER catalysis by attaching Ni foam (1.4 mm thick) on the flat Ni foil at the photocathode surface (by using Ni-filled epoxy). The 3D structure of the applied Ni foam offered a higher active surface area compared with the flat foil, which should be conducive to better HER catalysis of the photocathode. This has been shown elsewhere,[19–21] and was confirmed herein by the *j–V* measurement presented in Figure S8 (Supporting Information), proving a shift of the onset potential for the cathodic current density in the anodic direction as well as the steeper slope in the *j–V* characteristics of the Ni foam compared with a Ni foil electrode. These results were reflected in the linear sweep curves shown in Figure 5, as the fill factor of the photocathode (filtered) increased significantly, indicating enhanced kinetics of the HER. As a consequence, the photocurrent density at the crossing point of the HER and OER curves was increased up to 4.6 mA cm^{-2}.

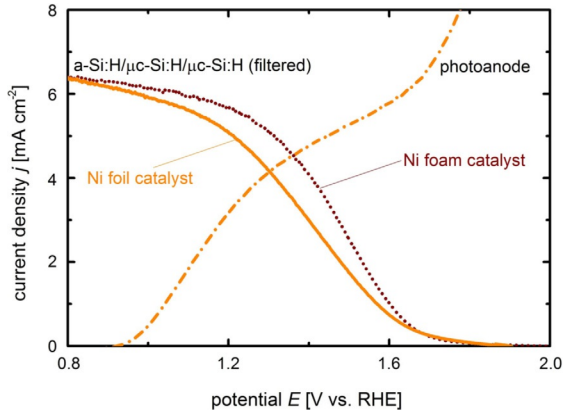

Figure 5. Linear-sweep measurement of the a-Si:H/μc-Si:H/μc-Si:H (with hematite filter) photocathode and the hematite photoanode (orange dotted curve) under 300 mW cm^{-2} illumination intensity. The linear-sweep measurement of the photocathode was performed with a flat Ni foil catalyst (orange solid curve) and a 3D Ni foam catalyst (dark red dotted curve). All measurements were conducted in 1 M NaOH electrolyte solutions using a Ag/AgCl reference electrode (3 M KCl).

Operation stability of hybrid tandem device

To confirm the results from Figure 5, obtained in the three-electrode configuration, we connected the hematite photoanode electrically to the a-Si:H/μc-Si:H/μc-Si:H/Ni photocathode, as shown in Scheme 1, and measured the bias-free photocurrent density of the hybrid tandem device in two-electrode configuration under 300 mW cm^{-2} illumination intensity. As apparent from Figure 6, the hematite/thin-film silicon PEC device exhibited unassisted solar water splitting with stable operation over more than 24 h. In the first period of operation, a bias-free photocurrent density of 4.6 mA cm^{-2} was measured, as estimated from the three-electrode measurements in Figure 5.

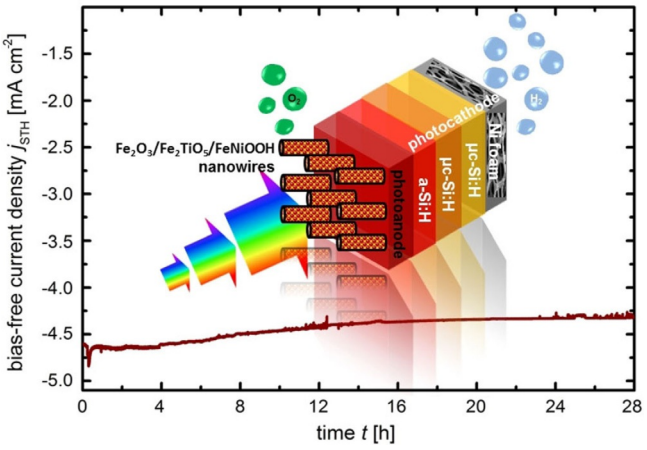

Figure 6. Net bias-free photocurrent density of the hybrid hematite/thin-film silicon tandem device under 300 mW cm^{-2} illumination intensity in 1 M NaOH electrolyte solution. The measurement was conducted over more than 24 h operation. The inset gives a schematic depiction of the hybrid tandem configuration under operation.

After 28 h continuous PEC-WS operation, the hybrid tandem device showed good robustness, and 94% of the initial bias-free photocurrent density was retained (4.3 mA cm^{-2}). Referring to the state-of-the-art oxide-based PEC-WS devices in the literature, this is an outstanding bias-free photocurrent density, outperforming similar tandem device approaches, which usually operate at current densities below 1 mA cm^{-2} (for 1 sun illumination intensity) and use noble-metal catalysts.[7–9,22–29] Table S2 (Supporting Information) summarizes recent studies on hybrid tandem devices for unassisted water splitting. A long-term stability test confirmed that the Ni foil/Ni foam catalyst structure, as well as the hematite nanowire structures, ensured excellent protection of the photocathode and photoanode in harsh basic solutions (1 M NaOH), respectively. Figure 7 provides evidence that the nanowire multilayer composition, that is, the hematite core with the pseudobrookite protective coating, was intact after the 28 h stability test. From the HRTEM image of a nanowire edge in Figure 7a and the corresponding FFT spectrum in Figure 7b, the two indicated material phases could be deduced. Figure 7c depicts the corresponding IFFT RGB composition map of the HRTEM image (Fig-

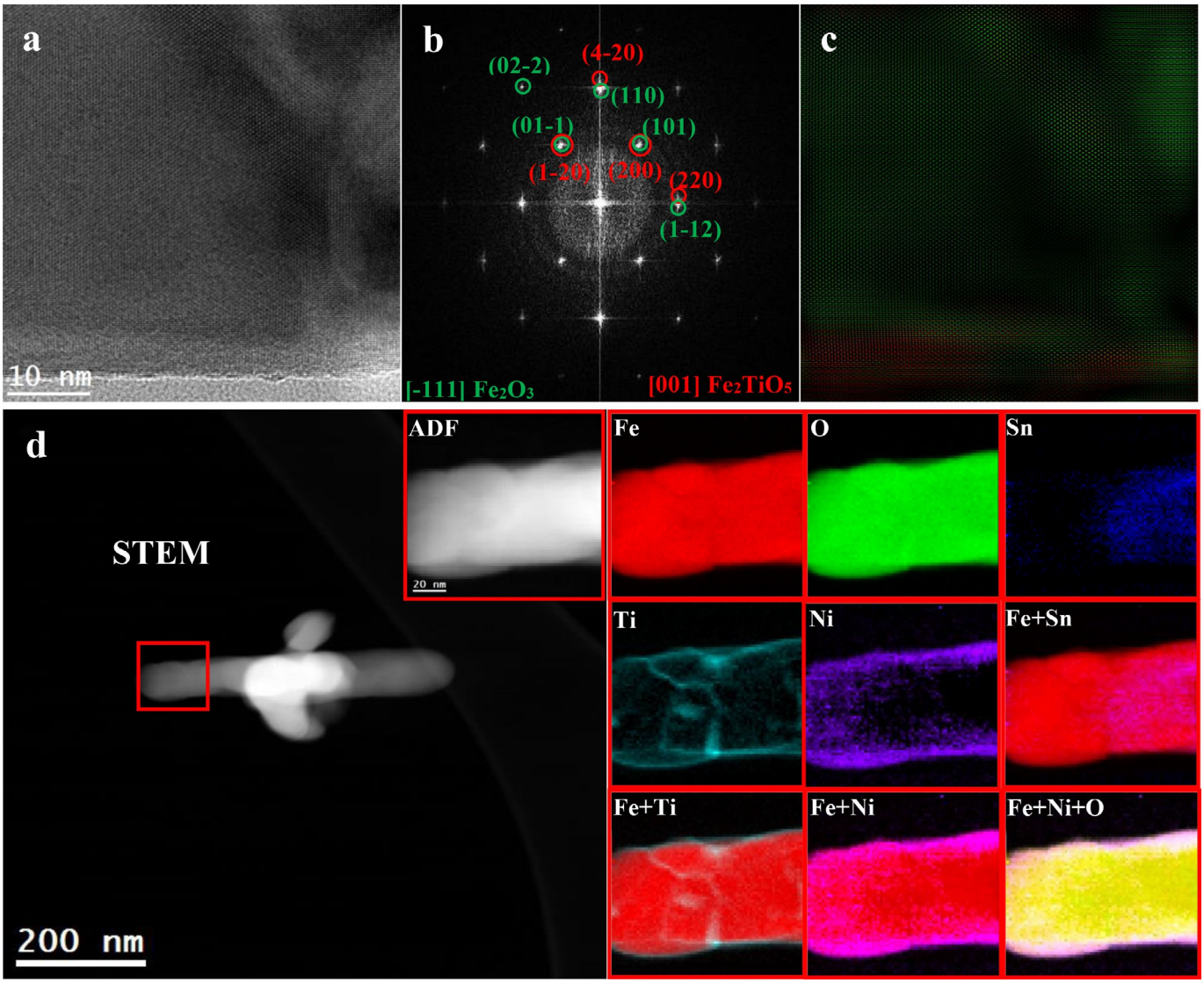

Figure 7. a) High-resolution TEM image of a hematite nanowire after the 28 h operation stability test (Figure 6) area showing the hierarchal structure of the nanowire composite. b) Corresponding FFT spectrum of (a), indicating that the nanowire is composited of hematite and pseudobrookite visualized along the [−111] and [001] directions, respectively. c) Phase map obtained from (a) after mask filtering the corresponding spots for each of the phases in (b) and obtaining their corresponding IFFT RGB composite image. d) EELS chemical composition maps obtained from the red rectangle area of the annular dark-field (ADF)-STEM micrograph (left), showing a multilayer nanowire (after the stability test). Individual Fe (red), O (green), Sn (blue), Ti (indigo), and Ni (purple) maps and their composite.

ure 7 a), showing the Fe_2O_3 core and the Fe_2TiO_5 surrounding layer. The FeNiOOH nanoparticles also showed excellent robustness, as they could be detected on the pseudobrookite surface after the stability test, as shown by the EELS signals in Figure 7 d (lower right map) and in the TEM and HRTEM analysis in Figure S9 (Supporting Information). Furthermore, the EELS maps of the photoanode nanostructure before and after the stability test were in perfect agreement (Figure S2 versus Figure 7 d), which confirmed its high robustness.

Consequently, the slight observable decrease in the bias-free photocurrent density in Figure 6 (less than 6% over 28 h operation) presumably originated from degradation of the photocathode. One critical point to consider is the heating up of the photocathode. In continuous operation with concentrated illumination, the temperature of the photocathode will inevitably increase, which, in general, will result in a slight decrease in the photovoltage owing to changes in the bandgap energies of the thin-film silicon absorber layers.[15,30] This effect might have shifted the operation point of the hybrid PEC-WS device into a lower current-density region. Another possible explanation would be that light-induced degradation (LID) of the thin-film silicon material could have affected the long-term performance of the photocathode.[31] It is well accepted that LID could decrease the performance of thin-film silicon devices. Studies have shown that, in particular, the fill factor of the device is negatively affected, which would be to the detriment of the operation point of the hybrid tandem device. Nevertheless, it was shown that the effect of LID is less pronounced for μc-Si:H than for a-Si:H layers, which is why a-Si:H/μc-Si:H/μc-Si:H structures are less affected by LID than a-Si:H/a-Si:H/μc-

Si:H or a-Si:H/a-Si:H multijunctions, having two a-Si:H absorber layers.[31]

Discussion

The laboratory-scale device presented in this study was designed from components that can be scaled up to larger PEC-WS systems. Furthermore, only earth-abundant materials (absorbers and catalysts) were applied, which potentially enable the deployment of economical large-scale installations. Nevertheless, foregoing the use of noble metal catalysts (e.g., Pt or RuO_2) and expensive photovoltaic structures (e.g., multijunction III–V group elements) inevitably implies limitations in the electrochemical reaction kinetics and achievable photocurrents, respectively. To circumvent this tradeoff for PEC-WS between economic viability and high-yield H_2 production, the concept of light concentration proposed herein might be of significant interest. In particular, tandem systems can profit from light concentration approaches, because in this case, both absorber layers benefit from the increased light intensity boosting the operative photocurrent density even more than in decoupled photoanode–cathode or anode–photocathode systems, respectively, in which the performance of only one component would be enhanced.

Nevertheless, it should be noted that the presented analysis (as well as the majority of the related studies) assumes that the concentrated light on the hybrid tandem device cell is the only energy input into the system. In reality, however, there can be additional energy inputs, including the energy required to flow the electrolyte continuously (e.g., for gas bubble removal) and heat management. For large-scale concentrated PEC-WS devices there may also be optical losses in the lenses or mirrors used to concentrate the incident sunlight onto the light absorber, which could reduce the system efficiency. In fact, we chose to neglect these aspects in our investigation, for two main reasons: 1) for the sake of comparison with results from previous studies; and 2) because the losses in a laboratory-scale demonstration system are less relevant, in addition to being more difficult to quantify accurately. As a result, the bias-free photocurrent reported herein represents a limiting upper bound with respect to any additional auxiliary energy inputs that would be required for any commercially scaled concentrated PEC-WS system.

Moreover, the backward reaction, that is, the recombination of hydrogen and oxygen into water, can impair the overall STH efficiency. The next immediate step would therefore be to implement a gas separation membrane for the upscaled design, such as that reported by Verlage et al.[32] In this regard, the addition of carbonate salts or other electron mediators in the electrolyte could also prevent the backward reaction and thereby enhance the hydrogen production rate.[33,34]

Overall, the goal of every solar-driven H_2 generation system is to minimize the levelized cost of hydrogen produced over the operating lifetime of the system. Although the photocurrent densities achieved with the presented hybrid tandem device are low compared with decoupled EC-PV systems,[35] the low-cost and scalable approach that this strategy offers may have the potential to produce hydrogen at an equivalent cost. Furthermore, considering a sort of "PEC farm" comprising many upscaled PEC-WS devices for H_2 production, the lower photocurrent densities could be beneficial in terms of lower overpotential losses, and thus, may actually lead to higher overall efficiencies. In this regard, it is projected by techno-economic models of large-scale, centralized solar H_2 production facilities that overpotential losses at high operating current densities are one of the most important factors in reducing the STH efficiency, and therefore, in increasing the cost of H_2.[36,37] Therefore, continued development of more efficient optical coupling of hybrid tandem partners by tuning of the functional layers and sub-cell currents, and technoeconomic models to predict hydrogen costs, are all important subjects for continuing research in the field of PEC-WS.

Conclusions

We have presented an efficient and scalable approach for photoelectrochemical water splitting (PEC-WS), which only makes use of low-cost and earth-abundant absorber and non-noble catalyst materials. The concept of light concentration was successfully introduced for hybrid devices for solar hydrogen production, which could effectively increase the bias-free photocurrent density, and thus, the solar-to-hydrogen (STH) efficiency of the dual-absorber tandem device (which was increased by 27%). In the optimized PEC-WS device configuration, a bias-free photocurrent density of 4.6 mA cm^{-2} was achieved over a prolonged period of operation (28 h). In conclusion, this study can serve as proof of concept that the promises of oxide-based devices for solar water splitting, regarding price, photocurrents, and stability, can be fulfilled, keeping PEC-WS on course as a viable alternative to other pathways for solar hydrogen production.

Acknowledgements

The authors acknowledge funding from Generalitat de Catalunya through the CERCA program, 2017 SGR 1246, 2017 SGR 327 and the Spanish MINECO projects MAT2014-59961, ENE2016-80788-C5-5-R and ENE2017-85087, together with the support from REPSOL, S. A. ICN2 is supported by the Severo Ochoa program from Spanish MINECO (Grant No. SEV-2017-0706). IREC also acknowledges additional support from the European Regional Development Funds (ERDF, FEDER), (S)TEM part of the present work has been performed in the framework of Universitat Autònoma de Barcelona Materials Science PhD program and the rest in the Nanoscience program of the University of Barcelona. The authors thank S. Moll (IEK-5), M. Biset-Peiró (IREC), and H. Xie (IREC) for their contribution to this work. F.U. acknowledges financial support from MINECO through Juan de la Cierva fellowship (FJCI-2016–29147).V.S., K.W., and F.F. (authors from IEK-5) thank the Deutsche Forschungsgemeinschaft (DFG) (Priority Program SPP 1613).

Conflict of interest

The authors declare no conflict of interest.

Keywords: hematite · silicon · tandem devices · thin films · water splitting

[1] T. J. Jacobsson, *Energy Environ. Sci.* **2018**, *11*, 1977.
[2] M. R. Shaner, H. A. Atwater, N. S. Lewis, E. W. McFarland, *Energy Environ. Sci.* **2016**, *9*, 2354.
[3] S. Dahl, I. Chorkendorff, *Nat. Mater.* **2012**, *11*, 100.
[4] A. C. Nielander, M. R. Shaner, K. M. Papadantonakis, S. A. Francis, N. S. Lewis, *Energy Environ. Sci.* **2015**, *8*, 16.
[5] K. Sivula, F. Le Formal, M. Grätzel, *ChemSusChem* **2011**, *4*, 432.
[6] P. Tang, H. Xie, C. Ros, L. Han, M. Biset-Peiró, Y. He, W. Kramer, A. P. Rodríguez, E. Saucedo, J. R. Galán-Mascarós, T. Andreu, J. R. Morante, J. Arbiol, *Energy Environ. Sci.* **2017**, *10*, 2124.
[7] F. Urbain, V. Smirnov, J.-P. Becker, A. Lambertz, F. Yang, J. Ziegler, B. Kaiser, W. Jaegermann, U. Rau, F. Finger, *Energy Environ. Sci.* **2016**, *9*, 145.
[8] J.-W. Jang, C. Du, Y. Ye, Y. Lin, X. Yao, J. Thorne, E. Liu, G. McMahon, J. Zhu, A. Javey, J. Guo, D. Wang, *Nat. Commun.* **2015**, *6*, 7447.
[9] P. Xu, J. Feng, T. Fang, X. Zhao, Z. Li, Z. Zouab, *RSC Adv.* **2016**, *6*, 9905.
[10] N. Kornienko, N. A. Gibson, H. Zhang, S. W. Eaton, Y. Yu, S. Aloni, S. R. Leone, P. Yang, *ACS Nano* **2016**, *10*, 5525.
[11] F. Urbain, K. Wilken, V. Smirnov, O. Astakhov, A. Lambertz, J.-P. Becker, U. Rau, J. Ziegler, B. Kaiser, W. Jaegermann, F. Finger, *Int. J. Photoenergy* **2014**, 249317.
[12] F. Urbain, V. Smirnov, J.-P. Becker, U. Rau, F. Finger, J. Ziegler, B. Kaiser, W. Jaegermann, *J. Mater. Res.* **2014**, *29*, 2605.
[13] B. Iandolo, B. Wickman, I. Zorić, A. Hellman, *J. Mater. Chem. A* **2015**, *3*, 16896.
[14] A. Royne, C. J. Dey, D. R. Mills, *Sol. Energy Mater. Sol. Cells* **2005**, *86*, 451.
[15] F. Urbain, S. Murcia-López, N. Nembhard, J. Vázquez-Galván, C. Flox, V. Smirnov, K. Welter, T. Andreu, F. Finger, J. R. Morante, *J. Phys. D* **2019**, *52*, 044001.
[16] D. Klotz, D. S. Ellis, H. Dotan, A. Rothschild, *Phys. Chem. Chem. Phys.* **2016**, *18*, 23438.
[17] I. A. Yunaz, A. Yamada, M. Konagai, *Jpn. J. Appl. Phys.* **2007**, *46*, 45.
[18] Y. Pihosh, I. Turkevych, K. Mawatari, J. Uemura, Y. Kazoe, S. Kosar, K. Makita, T. Sugaya, T. Matsui, D. Fujita, M. Tosa, M. Kondo, T. Kitamori, *Sci. Rep.* **2015**, *5*, 11141.
[19] J. Lu, T. Xiong, W. Zhou, L. Yang, Z. Tang, S. Chen, *ACS Appl. Mater. Interfaces* **2016**, *8*, 5065.
[20] B. Turan, J.-P. Becker, F. Urbain, F. Finger, U. Rau, S. Haas, *Nat. Commun.* **2016**, *7*, 12681.
[21] F. Urbain, P. Tang, N. M. Carretero, T. Andreu, L. G. Gerling, C. Voz, J. Arbiol, J. R. Morante, *Energy Environ. Sci.* **2017**, *10*, 2256.
[22] P. Bornoz, F. F. Abdi, S. D. Tilley, B. Dam, R. van de Krol, M. Graetzel, K. Sivula, *J. Phys. Chem. C* **2014**, *118*, 16959.
[23] F. Jiang, Gunawan, T. Harada, Y. Kuang, T. Minegishi, K. Domen, S. Ikeda, *J. Am. Chem. Soc.* **2015**, *137*, 13691.
[24] H. Kaneko, T. Minegishi, M. Nakabayashi, N. Shibata, Y. Kuang, T. Yamada, K. Domen, *Adv. Funct. Mater.* **2016**, *26*, 4570.
[25] J. H. Kim, H. Kaneko, T. Minegishi, J. Kubota, K. Domen, J. S. Lee, *ChemSusChem* **2016**, *9*, 61.
[26] T. Higashi, H. Kaneko, T. Minegishi, H. Kobayashi, M. Zhong, Y. Kuang, T. Hisatomi, M. Katayama, T. Takata, H. Nishiyama, T. Yamada, K. Domen, *Chem. Commun.* **2017**, *53*, 11674.
[27] Y. Goto, T. Minegishi, Y. Kageshima, T. Higashi, H. Kaneko, Y. Kuang, M. Nakabayashi, N. Shibata, H. Ishihara, T. Hayashi, A. Kudo, T. Yamadaa, K. Domen, *J. Mater. Chem. A* **2017**, *5*, 21242.
[28] A. Iwase, A. Kudo, Y. Numata, M. Ikegami, T. Miyasaka, N. Ichikawa, M. Kato, H. Hashimoto, H. Inoue, O. Ishitani, H. Tamiaki, *ChemSusChem* **2017**, *10*, 4420.
[29] L. Pan, J. H. Kim, M. T. Mayer, M.-K. Son, A. Ummadisingu, J. S. Lee, A. Hagfeldt, J. Luo, M. Grätzel, *Nat. Catal.* **2018**, *1*, 412.
[30] F. Urbain, J.-P. Becker, V. Smirnov, J. Ziegler, F. Yang, B. Kaiser, W. Jaegermann, S. Hoch, A. Maljusch, U. Rau, F. Finger, *Mater. Sci. Semicond. Process.* **2016**, *42*, 142.
[31] F. Urbain, V. Smirnov, J.-P. Becker, F. Finger, *ACS Omega* **2016**, *1*, 832.
[32] E. Verlage, S. Hu, R. Liu, R. J. R. Jones, K. Sun, C. Xiang, N. S. Lewis, H. A. Atwater, *Energy Environ. Sci.* **2015**, *8*, 3166.
[33] M. Ni, M. K. H. Leung, D. Y. C. Leung, K. Sumathy, *Renewable Sustainable Energy Rev.* **2007**, *11*, 401.
[34] R. Abe, K. Sayama, H. Arakawa, *Chem. Phys. Lett.* **2003**, *371*, 360.
[35] J. Jia, L. C. Seitz, J. D. Benck, Y. Huo, Y. Chen, J. W. D. Ng, T. Bilir, J. S. Harris, T. F. Jaramillo, *Nat. Commun.* **2016**, *7*, 13237.
[36] B. M. Klahr, D. Peterson, K. Randolph, E. L. Miller, *ECS Trans.* **2017**, *75*, 3.
[37] J. H. Montoya, L. C. Seitz, P. Chakthranont, A. Vojvodic, T. F. Jaramillo, J. K. Nørskov, *Nat. Mater.* **2017**, *16*, 70.

Manuscript received: December 5, 2018
Revised manuscript received: January 10, 2019
Accepted manuscript online: January 11, 2019
Version of record online: February 27, 2019